The Dhaka University Journal of Earth and Environmental Sciences, Vol. 14 (1): 2025

Impact of Cyclones on the Sediment Dynamics and Coastal Morphology Changes in Bangladesh: A Comparative Study between Cyclone Sidr and Cyclone Mora

Md. Suvo Tamim and M. Shahidul Islam*

Department of Geography and Environment, University of Dhaka, Dhaka 1000, Bangladesh

Manuscript received: 06 March 2025; accepted for publication: 30 April 2025

ABSTRACT: The low-lying coastline of Bangladesh is highly vulnerable to tropical cyclones, which can cause extensive geomorphological changes and redistribute coastal sediments. This study investigates the differential impacts of two cyclones—Category-4 Cyclone Sidr (2007) and Category-1 Cyclone Mora (2017)—on sediment reworking and post-storm recovery at two distinct coastal sites: Kuakata (embayment with mangroves) and Sonadia Island (open, deltaic shoreline). Using sediment cores (n=16), we analyzed grain size distributions, geochemical properties (TOC, TN), and diatom assemblages to identify cyclone-induced overwash deposits and evaluate post-event accretion trends. At Kuakata, landward-thinning overwash layers (3–7 cm thick) composed of moderately sorted fine sand (101.8–149.5 µm, σ_ϕ=1.70–2.01) and mixed marine-freshwater diatoms extended up to 375 m inland, highlighting the effect of storm surge moderated by mangrove cover. In contrast, Sonadia exhibited laterally scattered and thicker deposits (2–7 cm) with coarser sand (206.0–258.3 µm, σ_ϕ=1.54–1.69), shaped by open topography and tidal reworking. Post-storm accretion rates were higher in Sonadia (up to 4.3 cm/year) than Kuakata (1.9 cm/year), driven by aeolian and fluvial processes. The findings underscore how cyclone intensity, coastal geomorphology, and vegetation jointly regulate sediment deposition and recovery. This research demonstrates the utility of sedimentological and microfossil proxies in reconstructing storm events and highlights the need for long-term coastal monitoring to enhance resilience planning under changing climate conditions.

Keywords: Cyclone Impact; Sediment Dynamics; Coastal Morphology; Overwash Deposits; Accretion Rates

INTRODUCTION

Due to the geographical settings, concave shaped shoreline, and shallow continental shelf, Bangladesh is extremely vulnerable to cyclone that results in significant alterations to its coastal morphology (Anwar et al., 2022; Islam and Peterson, 2008). The majority of these cyclones make landfall during pre-monsoon and post-monsoon periods (Ali, 1999). Among those, Cyclone Sidr and Cyclone Mora caused extensive damage to the coastal areas of southern and southeastern Bangladesh, respectively (MoFDM, 2008; IMD Mora Report, 2017). In general, these effects on coastal morphology occur primarily due to the combined influence of storm surges, severe winds, and inland floods caused by intense rainfall before and during storms (Coch, 1994).

The coastline structure is significantly influenced by sediments from three mighty rivers (Ganges-Brahmaputra-Meghna), as well as the effects of wave and tide action (Hussain and Khan, 2018). According to Hasan and Matin (2019), the position of the shoreline is always changing due to the action of erosion and deposition, with the central zone being most dynamic, the western zone experiencing erosion and eastern zone gaining land. Due to the near flat topography and proximity to the Bay of Bengal, coastal region of Bangladesh is always at risk to flooding and erosion during cyclone (Brammer, 2014). Moreover, the shallow bathymetry and funnel-like shape of the Bay of Bengal affect the formation of cyclones in Bangladesh (Wasimi, 2009). Fluvial materials carried from GBM estuary during cyclones temporarily settle in the near shore region of Bay of Bengal affecting marine ecosystems and coastal habitats (Sarwar and Woodroffe, 2013). The amount and type of sediment deposition varied based on the difference in cyclone strength and local topography (Tweel and Turner, 2012).

The surge induced overflowing water has the capacity to erode shorelines, change coastal landforms, and remove sediments (Tebaldi et al., 2012). Additionally, the surge-induced waves play a significant role in

*Corresponding author: M. Shahidul Islam

Email: shahidul.geoenv@du.ac.bd

DOI: https://doi.org/10.3329/dujees.v14i1.83028

eroding dunes, beaches and barrier islands (Dasgupta et al., 2009). These effects lead to the changes in coastal geographical features, retreat of shoreline and sediment deposition patterns (Tebaldi et al., 2012). The forceful action of winds generates waves and currents that erode sandy shorelines, causing damage to various sandy features and leading to the reshaping of beach formations (Coch, 1994; Gresham et al., 1991; Smith and Jackson, 1990). Consequently, a considerable amount of eroded sediments, including sand, silt, clay and debris, is deposited beyond the beach area depending on the strength of surge-induced waves and local topography (Hache, et al., 2021; Soria et al., 2018). The deposited sediments, referred to washover or overwash deposits (Bennington and Farmer, 2014; Donnelly, et al., 2006), remains after storm subsides, changing landscape and influencing coastal sedimentation patterns (Michels et al., 1998).

Understanding the nature and characteristics of past cyclonic events from sediment signature is an important area of investigation in coastal areas. Soria et al., (2018) has emphasized understanding the attributes and distribution of overwash deposits which is crucial for studying the sediment dynamics and their impact on coasts. Different sedimentary facies, geochemical tools, microfossil assessment and other analyses are used as an essential tool to figure out ancient cyclones. The field of study within earth sciences is known as Paleotempestology (Coined by Emanuel, 2003; Muller et al., 2017). As evidenced by a good number of research (*e.g.* Das et al., 2013; Haque et al., 2021; Lambert et al., 2008; Morton, et al., 2008; Nott et al., 2013; Soria et al., 2018 and Williams, 2009), various techniques have been used to identify the characteristics of overwash deposits. The present study has been conducted to understand the cyclone affected sediment dynamics and spatial changes in coastal landform regions of Bangladesh. Field investigations were carried out at Kuakata and Sonadia regions to assess the impact of past cyclones in sediment reworking and changes of coastal morphology.

STUDY AREAS

Kuakata and Sonadia were selected as study area based on the historical track, cyclone type and severity of cyclones that affected Bangladesh over the last two decades (Fig. 1). Kuakata is located at Kalapara Upazila in Patuakhali district of the southern part of Bangladesh (Fig. 2). This coastal town has a sandy beach with a length of 18 km (Bangladesh Tourism Board, 2023). Sandy beaches, dunes, tidal flats, mangrove forest, and estuarine systems are some of the geomorphological features found in Kuakata (Sikder et al., 2021). Kuakata was affected by Cyclone Sidr on November 15, 2007, which was the deadliest cyclone since 1991. It was a category-4 cyclone that made landfall on the southern part of Bangladesh, with wind speeds reaching 240 km/h (MoFDM, 2008; Islam et al., 2011; Paul, 2009). The cyclone accompanied surge led to severe flooding, beach erosion, soil erosion, sediment accretion, deforestation, and biodiversity loss (Deb and Ferreira, 2017; Haque et al., 2021; Paul, 2009). Our sampling site was in the southwestern part of Kuakata, locally known as Lebur Bon or Sunset Point, adjacent to the estuary of the Andamanik River. At this site, data from four boreholes were collected along a north-south transect 577 meters from the shoreline and from two boreholes 375 meters east-west along the shoreline at 79 meters (Fig. 2a).

Sonadia is a small near-shore island in the Bay of Bengal off the southeastern coast of Bangladesh near Cox's Bazar (Fig. 2b) and covers an area of 9.3 km² (Bangladesh Tourism Board, 2023). The island features sandy beaches, dunes, sandbars, mangroves, and dynamic estuarine systems (Antu et al., 2022; Hossain et al., 2023). On May 30, 2017, Category-1 Cyclone Mora made landfall in this region, causing heavy rainfall and storm surge (IMD Mora Report, 2017; Al Azad et al., 2018). Considering the track path of Cyclone Mora, data from four boreholes were collected along a north-south transect 528 meters from the shoreline in the southeastern part of the island (Fig. 2b). Compared to Kuakata, Sonadia is characterized by low-lying, open topography with fragmented vegetation, which influenced the nature of cyclone-induced sedimentation and overwash distribution observed in the core data.

In both locations, field investigations were conducted by vertically inserting 50 cm long PVC pipes into the ground to collect undisturbed sediment cores (50 cm deep). These cores were carefully sealed at both ends to preserve their stratigraphic integrity, then transported to the laboratory for analysis. These intact cores serve as the basis for sedimentological, geochemical, and diatom-based analyses to evaluate cyclone impacts on coastal sediment dynamics and morphological changes.

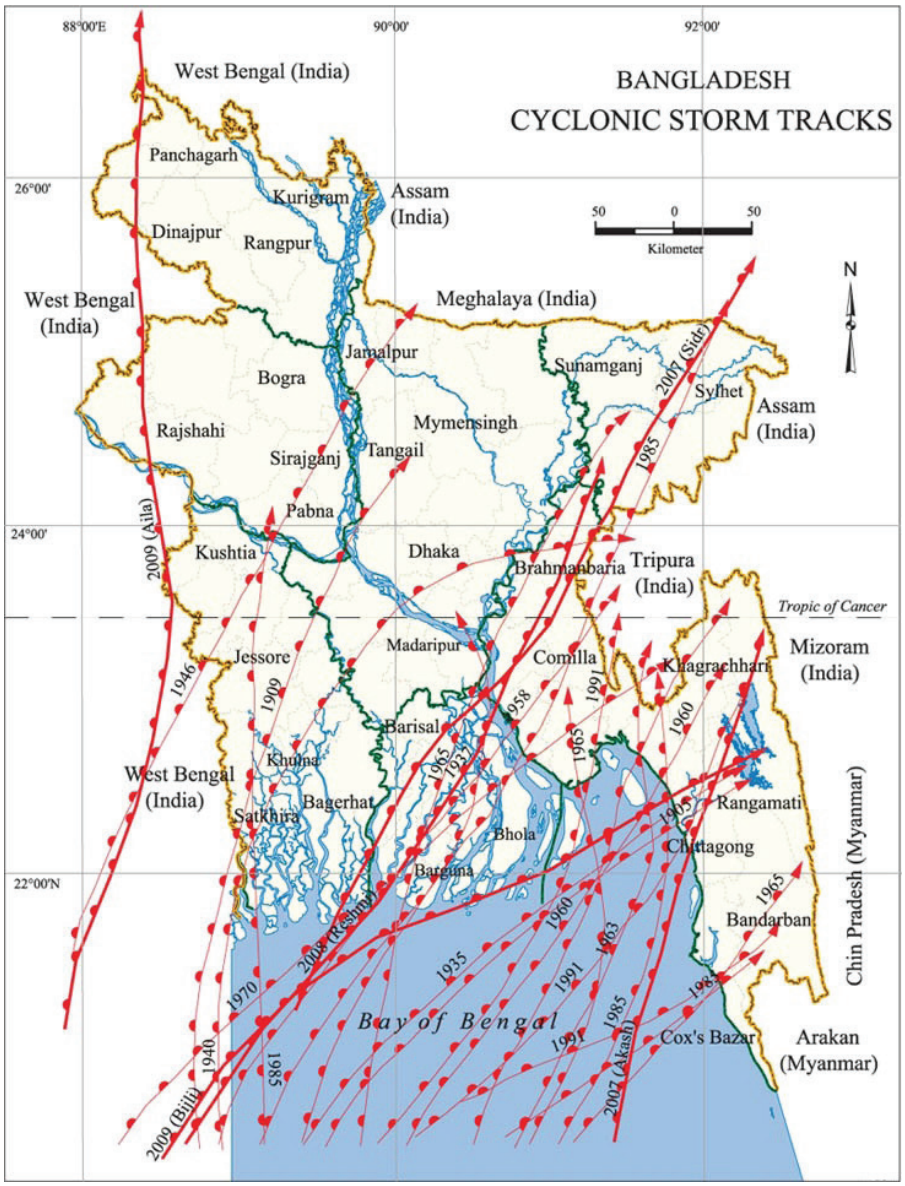

Figure 1: Map of Cyclonic Storm Paths of Bangladesh from 1900 to 2008 (Banglapedia, 2021)

METHODS

Field Investigation

Field surveys were conducted in both areas, and a total of nine boreholes were put down using 50 cm long PVC pipes. These pipes were inserted vertically into the ground with gentle manual pressure to obtain an undisturbed sediment profile. The sediment cores were retrieved by careful dissection of the pipes by a pipe-cutter at the workshop. The core samples were extracted precisely without damaging the soil profile for laboratory analysis. The aim of this sediment coring was to identify the sediments deposited due to the cyclonic events. The GPS values of all the sampling points were carefully recorded.

Laboratory Analysis

Sediment sub-samples from the cores were considered for laboratory analysis, such as particle size, geochemical properties, and diatom analysis, with an aim to trace the marker deposits drifted to the sample sites due to Cyclones Sidr and Mora. During the process, all necessary measures were taken to avoid any kind of contamination from outside

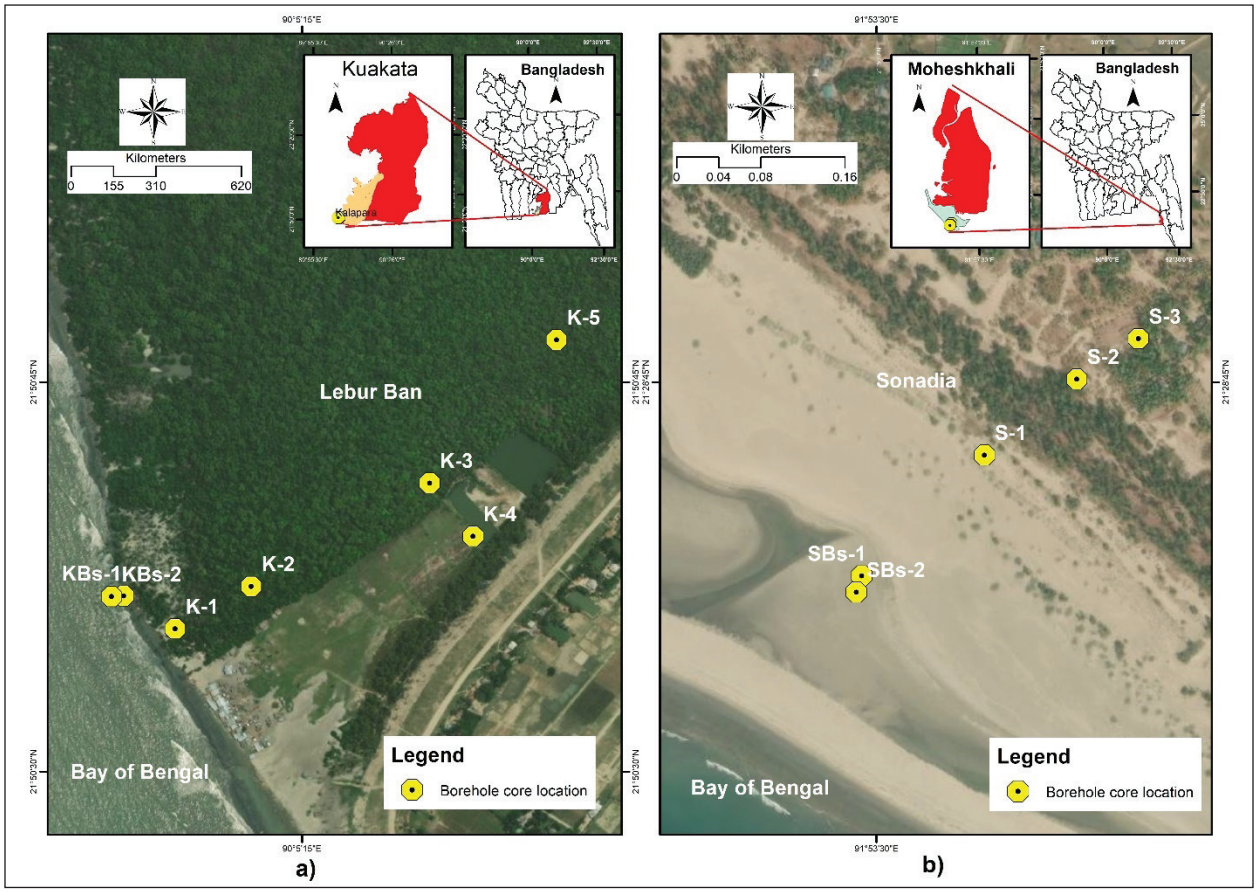

Figure 2: Maps Showing the Study Areas and Borehole Core Locations in (a) Kuakata and (b) Sonadia. This Figure Illustrates the Geographical Distribution of Sampling Sites Within the Two Coastal Regions

Particle Size Analysis

The particle size analysis was conducted using the dry sieve method for coarser sediments and the hydrometer method for finer sediments (Hossain et al., 2021a; Hossain et al., 2021b). Samples were first air-dried to remove all moisture content, and then 100 g of each sample was used for dry sieve analysis, while 50 g samples were used for hydrometer analysis. This process was carried out for 54 samples, taken at 10 cm intervals in each borehole, along with three additional samples from near the beach. Subsequently, the values obtained from the experiment were calculated using the Folk and Ward (1957) grain sorting (σ_ϕ) method, with the assistance of GRADISTAT Version 9.1 (Blott and Pye, 2001).

Geochemical Investigations

Total Organic Carbon (TOC) and Total Nitrogen (TN) content of sediments are crucial indicators for identifying unusual events in sediment layers, particularly those resulting from cyclonic events. In this study, TOC and TN were measured using the Walkley and Black (1934) method and the Kjeldahl (1883) method, respectively, as adapted from Huq and Alam (2005). A total of 57 samples were subjected to TOC analysis, similar to the particle size analysis, while TN analysis was performed on 12 samples from one borehole in Kuakata and one in Sonadia.

For TOC analysis, approximately 0.5 g of sieved soil was mixed with 10 ml of 1N potassium dichromate solution and 10 ml of concentrated sulfuric acid (98%) in a beaker. After cooling for 30 minutes, 150 ml of distilled water, 5 ml of phosphoric acid (85%), and diphenylamine indicator solution were added to the mixture. The mixture was then titrated with 1N ferrous sulfate solution. The volume of ferrous sulfate used was recorded, and a blank experiment was conducted without the soil sample.

For TN analysis, approximately 1 g of sieved soil, 20 ml of distilled water, and 25 ml of concentrated sulfuric acid were mixed in a Kjeldahl flask. After cooling for 20 minutes, the mixture was heated in a digestion chamber for 15 minutes until white fumes of H_2SO_4 appeared. A catalyst (2 g of a mixture of $CuSO_4 \cdot 5H_2O$ and anhydrous Na_2SO_4 in a 1:20 ratio) was added, and heating continued for over two hours until the liquid cleared and the soil turned light blue. After cooling, the digest was transferred to a 250 ml volumetric flask and filled to the mark with distilled water. The extract was distilled with 10 ml of 40% sodium hydroxide using Kjeldahl's distillation apparatus. A mixed indicator solution (0.5 g bromocresol green, 0.1 g methyl red, and 100 ml of 95% ethanol) and 10 ml of 4% boric acid were added to the distillate. The mixture was then titrated with standard H_2SO_4 until a pink color indicated the endpoint. A blank experiment was conducted simultaneously without soil.

Diatom Analysis

Diatoms are single-celled algae with cell walls composed of silica, which is resistant to chemical distortion. Diatoms are important markers for identifying sediment influx and reworking. In this study, diatom analysis was conducted using samples from two cores: core K-2 from Kuakata and core S-1 from Sonadia. A total of six samples from K-2 and another six from S-1 were analyzed, adapted from the method described by Islam and Tooley (1999).

For each sample, approximately 1 g of soil was placed in a 200 ml beaker. Twenty milliliters of 30% hydrogen peroxide (H_2O_2) were added to remove organic content from the sediments. The mixture was gently heated on a hot plate at approximately 80–90°C for 15-20 minutes until effervescence ceased. Two drops of 50% hydrochloric acid (HCl) were added to remove any remaining H_2O_2 and carbonates. The mixture was then centrifuged for 2 minutes at 1500 rpm. Most of the supernatant was decanted, leaving the remainder ready for slide mounting.

An 18x18 mm cover slip mounted on a glass slide was heated on a hot plate at approximately 70°C. Two to three drops of the sample, diluted with distilled water, were placed on the cover slip using a 1 ml pipette. After the liquid had completely evaporated and dried, a few drops of Naphrax were added. The cover slip was then inverted and gently heated to remove any remaining bubbles. Diatoms were counted at 400x magnification for standard identification and at 1000x for special identification, using a diatom catalog as a reference.

RESULTS

Site 1: Kuakata at Kalapara Upazila

Borehole records were analyzed using the Troels-Smith (1955) classification, revealing up to six distinct sedimentary layers that mark different depositional stages. In cores K-1, K-2, K-3, and K-4, distinct coarser sand intervals (3–7 cm thick) are evident, which can be interpreted as storm-derived overwash deposits. For example, core K-1—located 50 m from the shoreline—is predominantly composed of fine sand (average grain size ~133.9 μm) with parallel stratification. However, a sudden coarsening to 149.5 μm at 15–22 cm depth (Zone C, Fig. 4) is accompanied by moderately sorted sediment (σ_ϕ = 1.7). Similarly, core K-2 (144 m inland) shows six lithostratigraphic zones with a clearly demarcated coarser layer at 18 cm depth, resembling beach sand, and the presence of Keora (*Sonneratia apetala*) roots further confirms mangrove influence. In cores K-3 and K-4 (both at 375 m inland), abrupt increases in grain size occur at 29 cm (K-3; a 5 cm thick layer) and between 28–31 cm (K-4). In contrast, core K-5 (577 m inland) lacks such sudden changes, suggesting normal low-energy deposition (Table 1). Moreover, the observed decrease in overwash sediment thickness—from 7 cm in K-1 to 3 cm in K-4—highlights a clear spatial trend consistent with diminishing storm impact inland.

Geochemical measures further support the interpretation of overwash deposits. In core K-1, total organic carbon (TOC) and organic matter (OM) are low (averaging 0.3% and 0.29%, respectively), typical of well-oxygenated beach sands. Notably, at 20 cm depth (corresponding to Zone C), both TOC and OM increase modestly (0.6%), coinciding with the observed coarser sediment layer—suggesting the introduction of organic debris via storm surge. In core K-2, the finer average particle size (~70 μm) combined with higher TOC (0.56%) and OM (0.63%) values, along with poorer sorting (σ_ϕ = 2), point to a more dynamic depositional setting. Additionally, TOC/TN ratios in K-2, ranging from 2.19 to 6.13, fall within the typical range for marine sediments (3–10) and imply a mixed marine-terrestrial organic input, potentially influenced by tidal action (Meyers, 1997) (Fig. 3).

Table 1: Lithostratigraphic Description of Core K-1, K-2, K-3, K-4 and K-5 after Troels-Smith Scheme (1955)

K-1			K-2			K-3			K-4			K-5		
Layer No	Depth (cm)	Description	Layer No	Depth (cm)	Description	Layer No	Depth (cm)	Description	Layer No	Depth (cm)	Description	Layer No	Depth (cm)	Description
A	0-8	Sh^{+} Gs^{++} Ga^{3} As^{+} $nig.^{++}$ $sic.^{3}$ $strf.^{0}$ $elas.^{0}$ Ls? Grey to white fine sand	A	0-4	Sh^{++} Gs^{1} Ga^{3} Ag^{1} As^{1} $nig.^{2}$ $sic.^{2}$ $strf.^{0}$ $elas.^{1}$ Bluish grey silty sand	A	0-2	Sh^{+} Ld^{1} Gs^{2} Ga^{2} Ag^{1} As^{+} $nig.^{1}$ sic^{3} $strf.^{0}$ $elas.^{2}$ Light brownish grey Silty Sand	A	0-4	Sh^{++} Ld^{1} Gs^{2} Ga^{2} Ag^{1} As^{+} $nig.^{1}$ $sic.^{3+}$ $strf.^{0}$ $elas.^{1+}$ Light grey silty sand	A	0-2	Ld^{1} Gs^{2} Ga^{2} Ag^{1} As^{1} $nig.^{1}$ $sic.^{3}$ $strf.^{0}$ $elas.^{2}$ Ls? Light grey silty medium sand
B	8-15	Ga^{2} Nig^{+} $sic.^{4}$ $strf.^{1}$ $elas.^{0}$ Ls^{0} Dark grey fine sand	B	4-18	Gs^{1} Ga^{2} Ag^{3} As^{1} $nig.^{1++}$ $sic.^{1}$ $strf.^{0}$ $elas.^{2}$ Ls0 Dark bluish grey sandy silt	B	2-21	Same as layer A with some dark spot	B	4-17	Gs^{1} Ga^{2} Ag^{2} As^{1} $nig.^{1+}$ $sic.^{3}$ $strf.^{0}$ $elas.^{1}$ Ls^{4} Brownish grey silty sand	B	2-14	Sh^{+} Gs1 Ga^{2} Ag^{2} As^{1} $nig.^{2+}$ $sic.^{2+}$ $strf.^{1}$ $elas.^{1+}$ Ls^{0} Light grey silty fine sand with dark spot
C	15-22	Ga^{3} $nig.^{+}$ $sic.^{4}$ $strf.^{1}$ $elas.^{0}$ Ls^{0} White to grey fine sand	C	18-25	Sh^{++} Gs^{1} Ga^{3} Ag^{3} As^{1} $nig.^{+}$ sic^{2} $strf.^{1}$ $elas.^{0}$ Ls^{4} Silty Sand with a big root of *Sonneratia apetala*	C	21-29	Sh^{+} Gs^{2} Ga^{2} Ag^{2} As+ nig.1+ $sic.^{3}$ $strf.^{0}$ $elas.^{0}$ Ls^{0}	C	17-28	Gs^{2} Ga^{2} Ag^{2} As^{1} $nig.^{1+}$ $sic.^{2+}$ $strf^{0}$ $elas^{2}$ Ls^{0} Light brownish grey silty sand	C	14-21	Ld^{1} Gs^{1} Ga^{2} Ag^{2} As^{1} $nig.^{1}$ $sic.^{2}$ $strf.^{+}$ $elas.^{2}$ Ls^{0} Bluish grey silty fine Sand with roots
D	22-33	Sh^{+} Ga^{3} As^{++} $Nig.^{2}$ Sic^{4} $Strf^{1}$ $Elas^{0}$ Ls^{+} White to grey fine sand	D	25-30	Gs^{1} Ga^{3} Ag^{3} As^{1} $nig.^{2}$ $sic.^{3}$ $strf.^{1}$ $elas.^{0}$ Ls^{0} Light grey silty sand	D	29-34	Sh^{+} Gs^{2} Ga^{2} Ag^{1} As^{+} $nig.^{1}$ $sic.^{3}$ $strf.^{0}$ $elas.^{0}$ Ls^{0} Light-grey silty medium sand	D	28-31	Sh^{+} Gs^{2} Ga^{2} Ag^{1} As^{+} Nig^{2} $sic.^{2}$ $strf.^{0}$ $elas.^{2}$ Ls^{0} Dark grey silty sand	D	21-37	Ld^{1} Gs^{1} Ga^{2} Ag^{2} As^{1} $nig.^{1}$ $sic.^{2}$ $strf.^{+}$ $elas.^{2}$ Ls^{0} Reddish grey silty sand
E	33-50	$Ga2^{++}$ As^{+} Nig^{1} Sic^{4} $Strf^{2}$ $Elas^{0}$ Ls^{++} White to grey fine sand	E	30-43	Sh^{1} Gs^{1} Ga^{2} Ag^{2} As^{1} $nig.^{+}$ $sic.^{2}$ $strf.^{0}$ $elas^{2}$ Ls^{0} Silty sand with an organic layer and a root of unknown tree	E	34-50	Sh^{++} Gs^{2} Ga^{2} Ag^{1} As^{+} $nig.^{1}$ $sic.^{3}$ $strf.^{0}$ $elas.^{2}$ Ls^{0} Light grey silty sand with root	E	31-41	Sh^{++} Gs^{2} Ga^{2} Ag^{1} As^{+} Nig^{1} $sic.^{2}$ $strf.^{0}$ $elas.^{2}$ Ls^{0} Light grey silty sand	E	37-50	Gs^{1} Ga^{2} Ag^{3} As^{1} $nig.^{1}$ $sic.^{3}$ $strf.^{0}$ $elas.^{2}$ Ls^{0} Light grey sandy silt with roots
			F	43-50	Gs^{1} Ga^{2} Ag^{2} As^{1} $nig.^{2}$ $sic.^{3}$ $strf.^{0}$ $elas.^{2}$ Ls^{0} Silty sand with dark spot				F	41-50	Sh^{++} Gs^{2} Ga^{2} Ag^{1} As^{+} $nig.^{1}$ $sic.^{3}$ $strf.^{0}$ $elas.^{2}$ Ls^{0} Bluish silty medium sand			

Diatom analysis in core K-2 offers further corroboration of cyclone impacts. While freshwater diatoms—such as *Navicula retusa, Cavinula jaernefeltii, Diploneis ovalis*, and *Cymbella affinis*—comprise 68% of the assemblage overall, a pronounced surge in marine diatoms is observed at the 20 cm depth (Fig. 5). Here, the marine diatoms, notably *Coscinodiscus centralis*, account for 52% of the diatom population, coinciding with the coarser sandy layer (Zone C). The residual presence of freshwater diatoms (18%) at this depth may reflect simultaneous river flooding during the cyclone (Haque et al., 2021; Wang et al., 2019), while the overall diatom evidence aligns with cyclone occurrence as suggested by Heller et al. (2021).

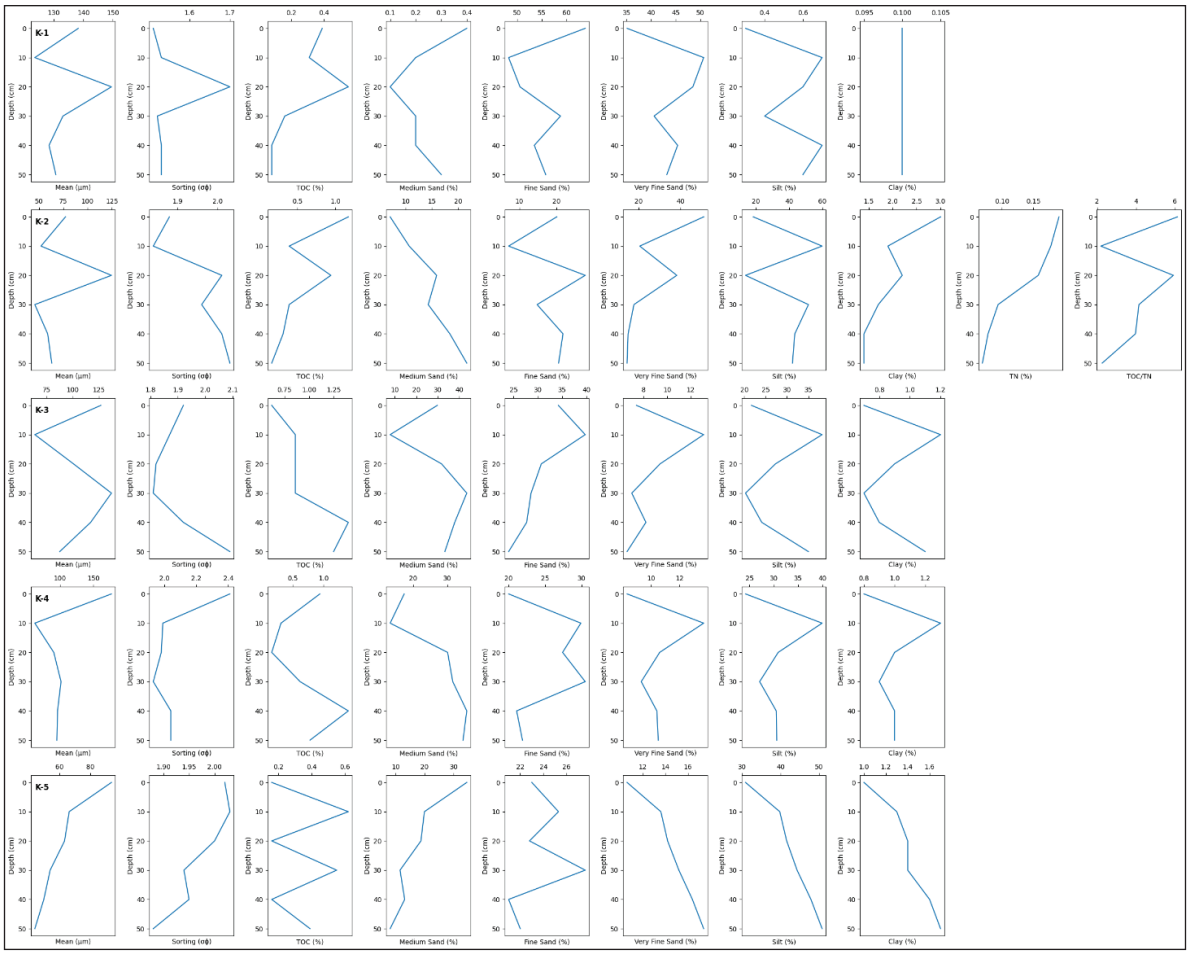

Figure 3: Mean Particle Sizes, Sorting, Geochemical Properties, and Size Distributions for each Sediment Layer within the Cores from the Kuakata Study area

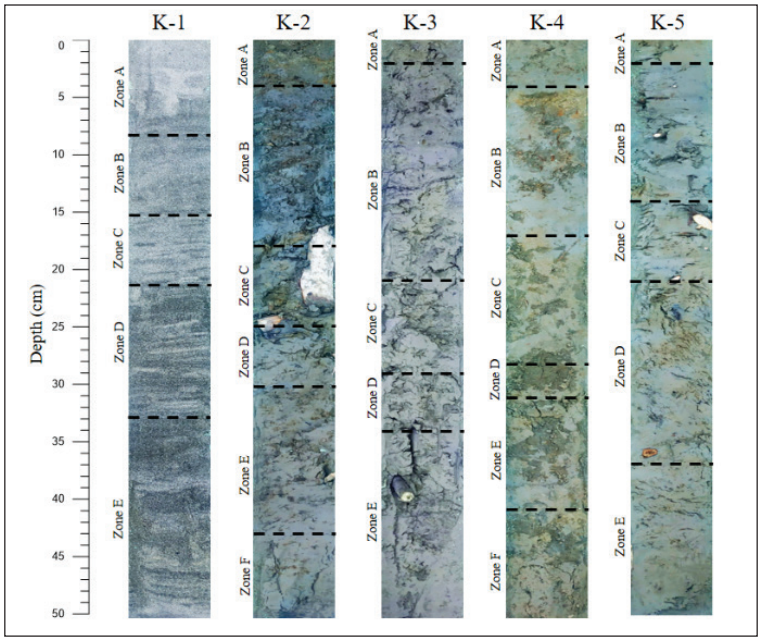

Figure 4: Photos of Core K-1, K-2, K-3, K-4 and K-5 Along with Their Respective Zones (The Stratigraphic Descriptions of These Cores are Detailed in Table 1)

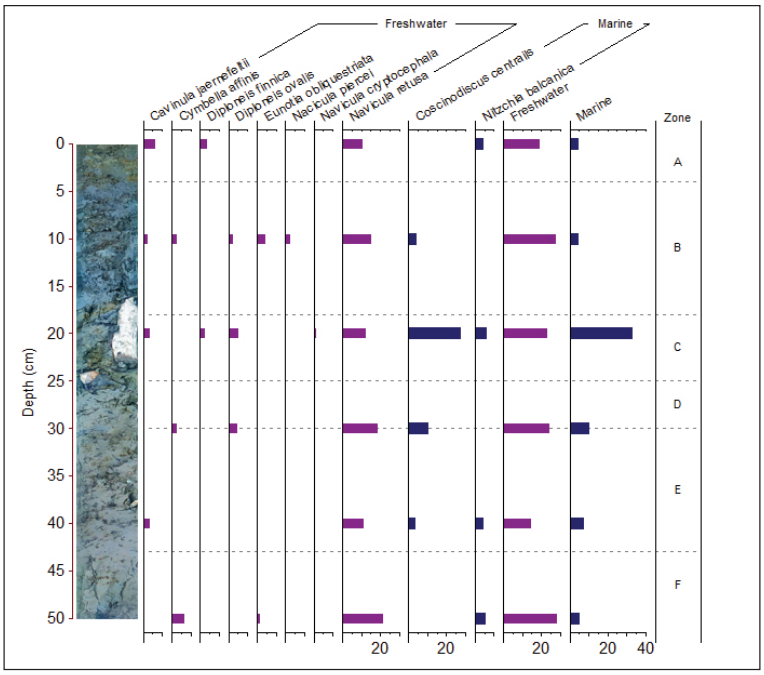

Figure 5: Diatom Analysis of Core K-2, Kuakata (The Stratigraphic Descriptions of the Zones of Core K-2 are Detailed in Table 1)

Site 2: Sonadia at Moheshkhali Upazila

Sediment cores from Sonadia Island reveal a more complex stratigraphy compared to Kuakata, with up to eight distinct sedimentary layers (Fig. 7). This complexity reflects the island's dynamic geomorphic evolution driven by high sediment accumulation from shoreline activities (Hossain et al., 2023), direct marine exposure (Hoque et al., 2022), and proximity to the Moheshkhali–Kutubdia Channel estuary and adjacent river delta (Hasan, 2020).

Core S-1, collected 148 meters from the shoreline, displays eight sedimentary layers with alternating reddish-brown and dark reddish-brown bands. The color variations—attributed to iron oxide enrichment and intermittent organic matter input—are further evidenced by the presence of mollusk shells in the uppermost layer, indicating strong marine influence near the coast. In contrast, cores collected further inland (S-2 at 263 m, S-3 at 319 m, and S-4 at 518 m) show a gradual transition in both texture and color. Core S-2 is dominated by light brown layers, with its uppermost (0–5 cm) dark brown band likely resulting from humification processes (Table 2). Core S-3 reintroduces reddish-brown and light-brown stratification, whereas core S-4, situated within a mangrove forest, exhibits only four dark gray layers dominated by silt.

Table 2: Lithostratigraphic Description of Core S-1, S-2, S-3 and S-4 after Troels-Smith Scheme (1955)

S-1			S-2			S-3			S-4		
Layer No	Depth (cm)	Description	Layer No	Depth (cm)	Description	Layer No	Depth (cm)	Description	Layer No	Depth (cm)	Description
A	0-6	Sh^{+} Gs^{1} Ga^{4} $nig.^{1}$ $sic.^{3}$ $strf.^{0}$ $elas.^{2}$ Ls? Dark reddish brown fine sand with *Mollusca* present	A	0-5	Sh^{1} Ld^{1} Gs^{3} Ga^{2} Ag^{1} $nig.^{2+}$ $sic.^{3}$ $strf.^{0}$ $elas.^{1+}$ $Ls^{?}$ Very dark brown medium sand	A	0-1	Sh^{1} Gs^{2} Ga^{3} Ag^{1} $nig.^{2+}$ $sic.^{3}$ $strf.^{0}$ $elas.^{1}$ Ls? Very sark Reddish brown sandy soil with 10^{o} slope in lower boundary	A	0-1	Gs^{1} Ga^{2} Ag^{3} As^{1} $nig.^{1+}$ $sic.^{2+}$ $strf.^{0}$ $elas.^{2}$ Ls? grey soft sandy silt

B	6-13	Gs^{1} Ga^{3} $nig.^{1+}$ $sic.^{3}$ $strf.^{1}$ $elas.^{1+}$ Ls^{+} Dark reddish brown fine sand with parallel laminae with 2° slope	B	5-14	Sh^{1} Gs^{3} Ga^{2} $nig.^{1+}$ $sic.^{2+}$ $strf.^{0}$ $elas.^{0}$ Ls^{0} Reddish brown medium sand with some roots	B	1-19	Sh^{++} Gs^{2} Ga^{3} $nig.^{2+}$ $sic.^{2+}$ $strf^{1}$ $elas.^{+}$ Ls^{+} Dark brown Sandy Soil with 2° slope in lower boundary	B	1-19	Gs^{1} Ga^{2} Ag^{3} As^{1} $nig.^{1+}$ $sic.^{2+}$ $strf.^{0}$ $elas.^{2}$ Ls^{4} sandy silt with unknown tree roots
C	13-23	Gs^{3} Ga^{2} $nig.^{1+}$ $sic.^{3}$ $strf.^{0}$ $elas.^{1+}$ Ls^{4} Reddish brown medium sand with 10° slope	C	14-24	Sh^{++} Gs^{3} Ga^{2} $nig.^{1}$ $sic.^{2+}$ $strf.^{+}$ $elas.^{0}$ Ls^{0} Light reddish brown medium sand	C	19-21	Sh^{++} Gs^{1} Ga^{4} $nig.^{1}$ $sic.^{3}$ $strf.^{+}$ $elas.+$ Ls^{4} Light brown sandy Soil	C	19-23	Gs^{1} Ga^{2} Ag^{3} As^{1} $nig.^{1+}$ $sic.^{2}$ $strf.^{0}$ $elas.^{2}$ Ls^{4} Dark grey sandy silt
D	23-29	Gs^{3} Ga^{2} $nig.^{2+}$ $sic.^{3}$ $strf.^{0}$ $elas.^{1+}$ Ls^{4} Dark Brown Medium Sand with 10° slope in upper boundary and 15° slope in lower boundary	D	24-31	Sh^{++} Gs^{3} Ga^{2} $nig.^{1+}$ $sic.^{2+}$ $strf.^{+}$ $elas.^{0}$ Ls^{0} Light brown medium sand	D	21-29	Sh^{1} Gs^{4} $nig.^{1+}$ $sic.^{3}$ $strf.^{2}$ $elas.^{0}$ Ls^{4} Parallel assemblage of dark brown sandy soil and light brown sandy soil	D	23-30	Sh^{++} Gs^{2} Ga^{2} Ag^{2} As^{1} $nig.^{2}$ $sic.^{2}$ $strf.^{0}$ $elas.^{2}$ Ls^{+} Dark grey silty sand
E	29-34	Sh^{+} Gs^{4} Ga^{1} $nig.^{2+}$ $sic.^{3}$ $strf.^{1}$ $elas.^{1+}$ Ls^{4} Reddish brown medium sand	E	31-38	Same as layer F $nig.^{1}$	E	29-42	Sh^{+} Gs^{3} Ga^{2} $nig.^{1}$ $sic.^{3}$ $strf.^{2}$ $elas.^{0}$ Ls^{4} Light brown sandy soil			
F	34-40	Same as layer B with 15° slope in lower boundary	F	38-41	Sh^{1} Gs^{3} Ga^{2} Ag^{1} $nig.^{1+}$ $sic.^{3}$ $strf.^{+}$ $elas.^{0}$ Ls^{+} Medium sand with some silt with 40° slope in lower boundary	F	42-46	Same as layer G $nig.^{2}$ dark brown sandy soil			
G	40-43	Sh^{+} Gs^{2} Ga^{3} $nig.^{1}$ $sic.^{2+}$ $strf.^{1}$ $Elas^{1}$ Ls^{+} Light brown fine sand	G	41-50	Sh^{+} Gs^{3} Ga^{2} $nig.^{1}$ $sic.^{3}$ $strf.^{0}$ $elas.^{+}$ Ls^{+} White to light brown medium sand	G	46-50	Sh^{+} Gs^{3} Ga^{2} $nig.^{1}$ $sic.^{3}$ $strf.^{2}$ $elas.^{0}$ Ls^{4} White to light brown sandy soil			
H	43-50	Gs^{2} Ga^{3} $nig.^{1}$ $sic.^{2+}$ $strf.^{1}$ $elas.^{1}$ Ls^{+} Dark brown fine sand with dark spot									

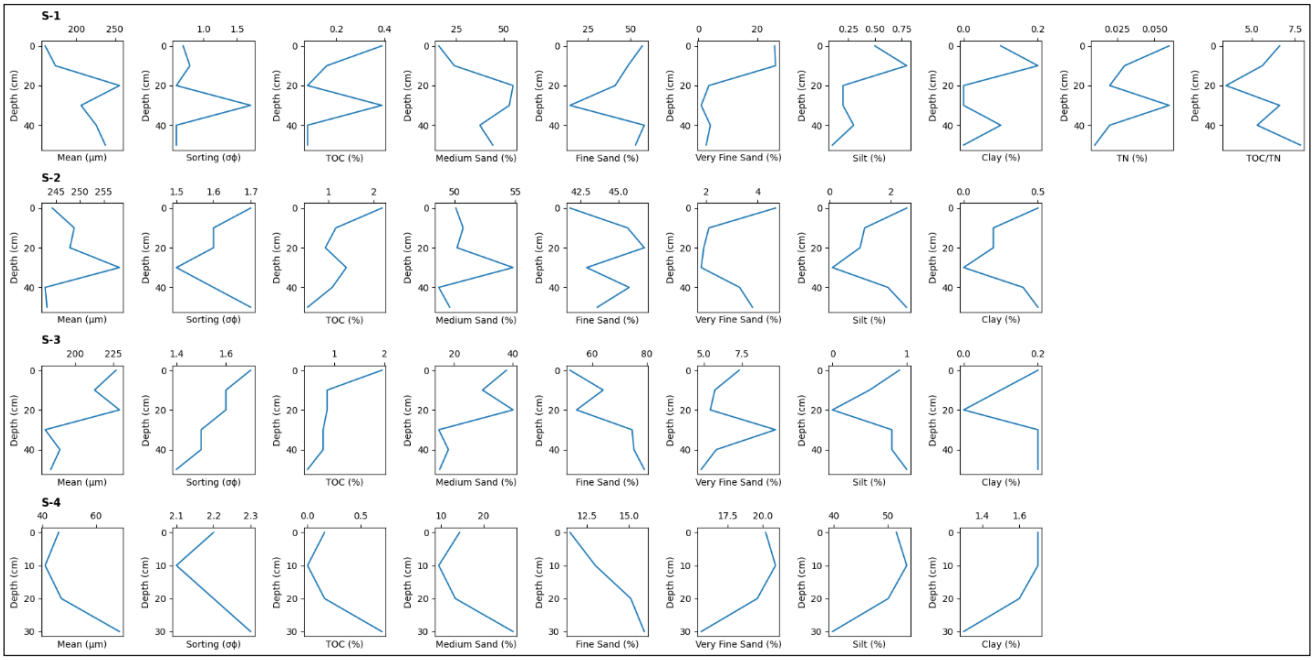

Figure 6: Mean Particle Sizes, Sorting, Geochemical Properties, and Size Distributions for each Sediment Layer within the Cores from the Sonadia Study area

The latter likely reflects a low-energy depositional environment where fine particles settle and organic matter from decomposing mangrove vegetation accumulates. Such a spatial trend—from marine-influenced, iron-rich sediments near the shoreline (S-1) to organic-rich, fine-textured deposits inland (S-2, S-3, S-4)—highlights the interplay between coastal processes and sediment delivery.

The sedimentary and geochemical properties (Fig. 6) further elucidate depositional dynamics. In core S-1, the average particle size (209.5 μm) is finer than that of local beach sand (267 μm); however, a marked increase to 255.9 μm at 30 cm depth (Zone E) is accompanied by a peak sorting value (σ_ϕ = 1.7) and elevated organic content (TOC: 0.39%; OM: 0.67%). These features indicate a dynamic depositional event, likely representing overwash sediments deposited during a high-energy cyclone. Additionally, TOC/TN ratios averaging 5.9 align with marine sediment signatures (Meyers, 1997), suggesting minimal terrestrial influence. In core S-2, the average particle size (247.5 μm) is coarser—comparable to beach sand—with consistent moderate sorting (average σ_ϕ = 1.6) and higher organic carbon (average TOC = 1.22%) and organic matter (average OM = 2.11%) contents, reflecting the influence of vegetation. A distinct layer with coarser particles (258.3 μm) at 30 cm depth in S-2 is interpreted as an overwash deposit, potentially linked to cyclone-induced reworking. Core S-3 exhibits a mean particle size of 203.7 μm with a significant peak at 20 cm depth (229.0 μm) and a corresponding increase in the medium sand fraction (40.2%), indicating a change in depositional energy. In contrast, core S-4 is dominated by very fine particles (average 47.9 μm) with poor sorting (average σ_ϕ = 2.2), implying a deposition regime with stronger riverine than tidal influence and a reduced marine organic input.

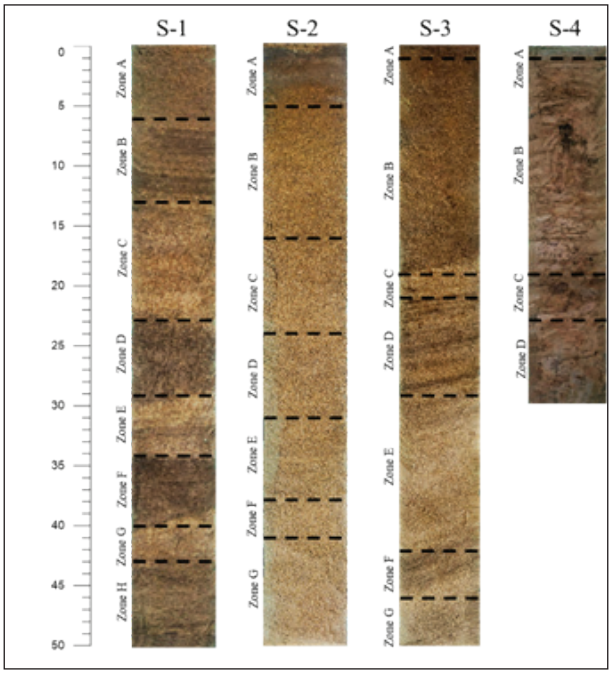

Figure 7: Photos of Core S-1, S-2, S-3 and S-4 Along with Their Respective Zones (The Stratigraphic Descriptions of These Cores are Detailed in Table 2)

Diatom analysis conducted on core S-1 provides additional support for the identification of overwash deposits. A total of eight diatom species were identified, including *Navicula cryptocephala, Diploneis ovalis*, and *Cymbella affinis* (Fig. 8). Although freshwater diatoms constitute a significant majority (85%) of the assemblage, a peak in diatom counts at 30 cm depth correlates with Zone E (Table 2; Fig. 7). This peak, in conjunction with the geochemical and textural evidence, suggests that a high-energy event—potentially linked to cyclone activity—transported both coarse sediment and organic debris inland. No diatoms were detected below 40 cm depth, which may reflect either reworking or conditions unfavorable for diatom preservation in deeper sediments.

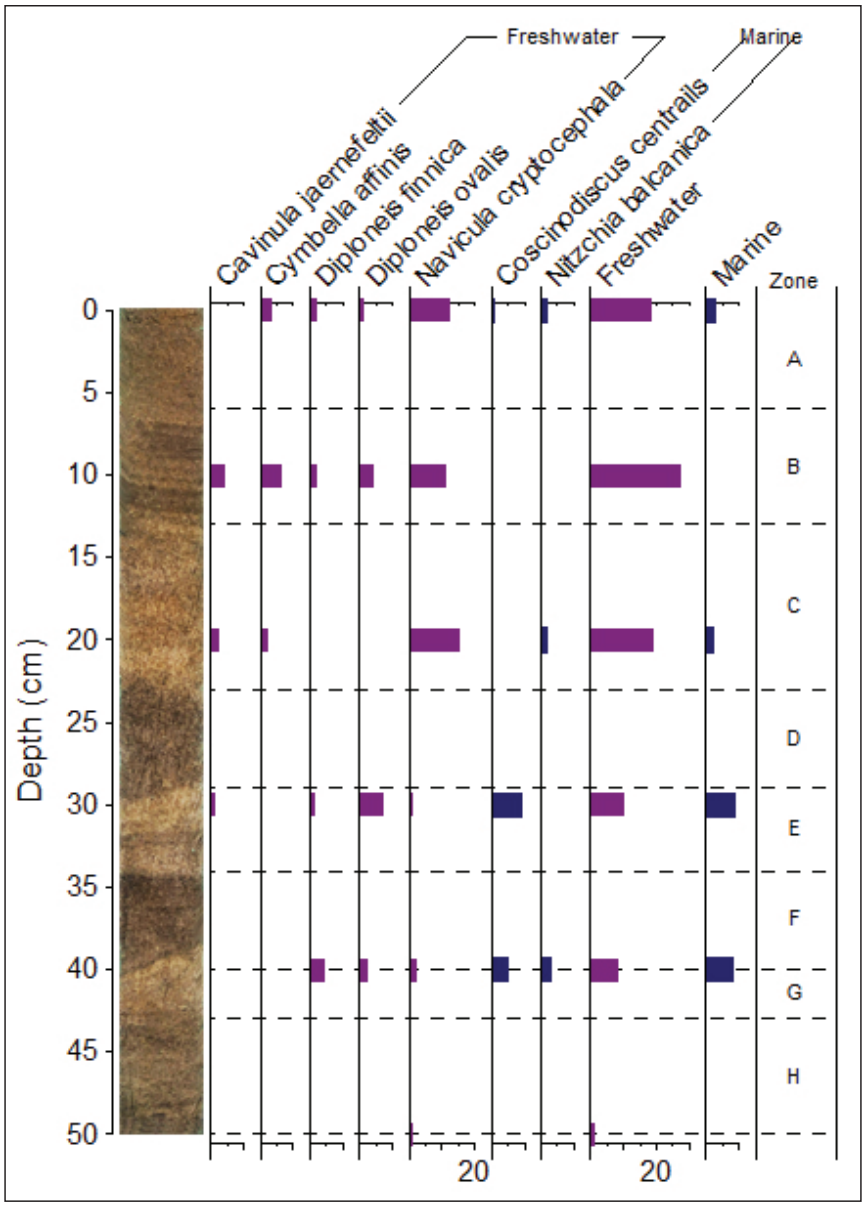

Figure 8: Diatom Analysis of Core S-1, Sonadia (The Stratigraphic Descriptions of the Zones of Core S-1 are Detailed in Table 2)

DISCUSSION

Comparative Insights into Overwash Deposition and Coastal Recovery

To examine cyclone-induced overwash deposition and subsequent recovery, nine sediment cores were obtained from two different coastal settings—Kuakata and Sonadia. By using extensive geochemical and biological examinations to illustrate how local geomorphology and vegetation influence sedimentary responses to cyclonic events.

Cyclone Sidr (2007), a storm with surges surpassing 12 m (Antony et al., 2014), has left a clear mark on the Kuakata region. Cores K-1 through K-4 have notable overwash deposits ranging in thickness from 3 to 7 cm, with the thickest layers observed in the nearshore cores (K-1 and K-2) (Fig. 9). Notably, these deposits occur at shallower depths in K-1 (within 20 cm) than in K-2 (30 cm) and K-3 (28 cm), owing to local topographic heterogeneity and influence of mangrove roots (Hawkes and Horton, 2012; Haque et al., 2021). The gradual inland thinning of these deposits, which is consistent with Hong et al. (2018) findings, demonstrates how

storm surge energy dissipates as it advances landward. Furthermore, the presence of mangrove root fragments in these cores reinforces the role of coastal vegetation in buffering storm impacts and contributing to organic matter accumulation, aligning with previous findings on erosion, deposition, and shoreline changes (*e.g.* Alam et al., 2018; Dufois et al., 2017; Hanebuth et al., 2013 and Shibayama et al., 2009).

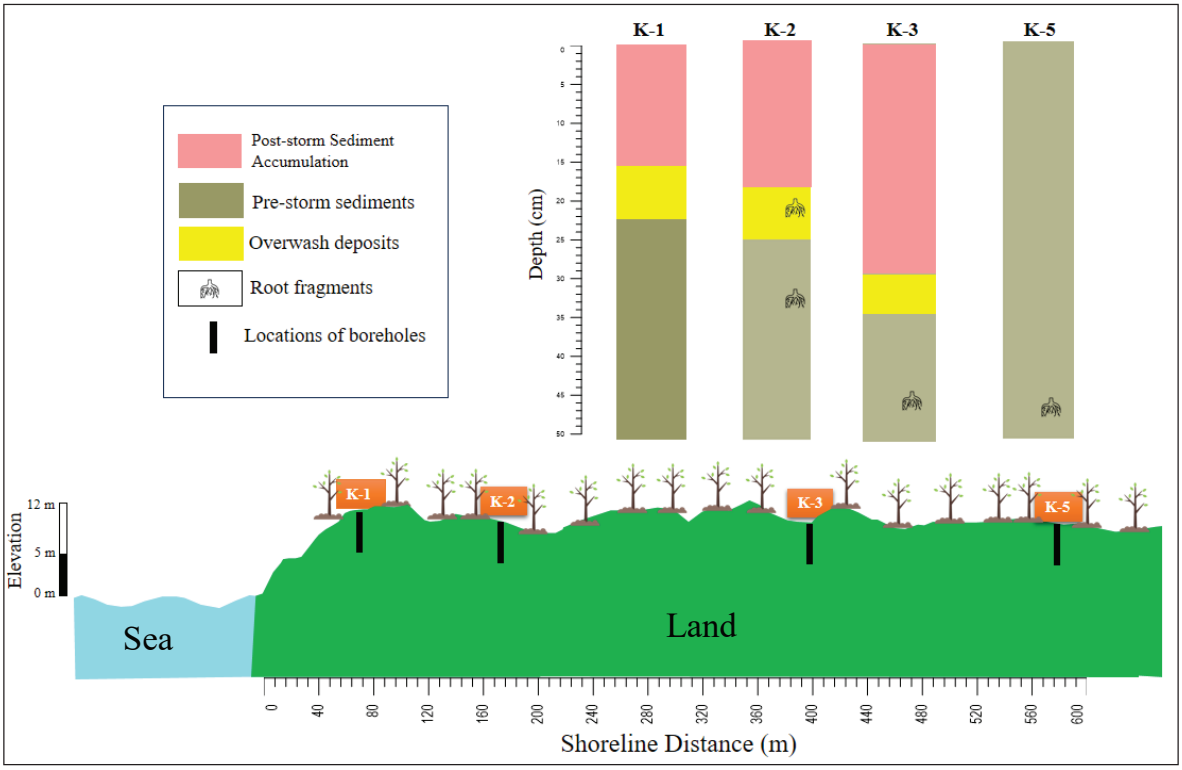

Figure 9: Schematic Representation of Over-wash sediments from cyclone Sidr based on Textural, Geochemical and Diatom Analysis

On the other hand, Sonadia Island, impacted by Cyclone Mora on May 30, 2017 (Paul, 2009; IMD Mora Report, 2017), has a significantly different overwash signature. The sedimentary record is more fragmented here, and overwash deposits do not show the same distinct landward-thinning pattern as Kuakata. Core S-1 contains a coarse sand layer (Zone E) with a peak particle size of 255.9 µm, elevated sorting (σ_ϕ = 1.7), and higher organic content (TOC: 0.39%; OM: 0.67%) at 30 cm depth (Fig. 10). The presence of mollusk shells layers (Kabir et al., 2018) emphasizes the marine influence near the shoreline, while the dominance of freshwater diatoms (85% in S-1) suggests riverine flooding caused by Mora's path through monsoon-swollen channels (Wang et al., 2019). By comparing these findings, the comparative analysis indicates that the extent and character of overwash deposition are influenced not just by storm strength, but also by local coastline configuration. The powerful surge from Cyclone Sidr pushed nearshore sediments further inland—up to 375 m—while the lower-intensity surge from Cyclone Mora in Sonadia resulted in more laterally distributed, discontinuous deposits due to the island's open, low-lying topography. These findings thus provide a necessity for doing broader paeleo-geomorphological study to understand how mangrove vegetation and estuarine proximity influence sediment dynamics, allowing for a more nuanced interpretation of post-cyclone recovery processes across various coastal environments in Bangladesh.

Spatial Variability and Sedimentation Dynamics

The Kuakata and Sonadia sediment records indicate marked spatial variation in overwash deposition, which is strongly controlled by local coastal morphology and hydrodynamic regimes. Overwash deposit mean particle sizes range from 101.8 to 149.5 µm in the Kuakata region, with a clear landward fining and moderately to poorly sorted sediments (1.70–2.01 σ_ϕ). Deposits here tend to be 3-7 cm thick (Table 3), a pattern similar to the findings of Haque et al. (2021) and consistent with the wave-energy dampening effect of embankments and mangrove canopy.

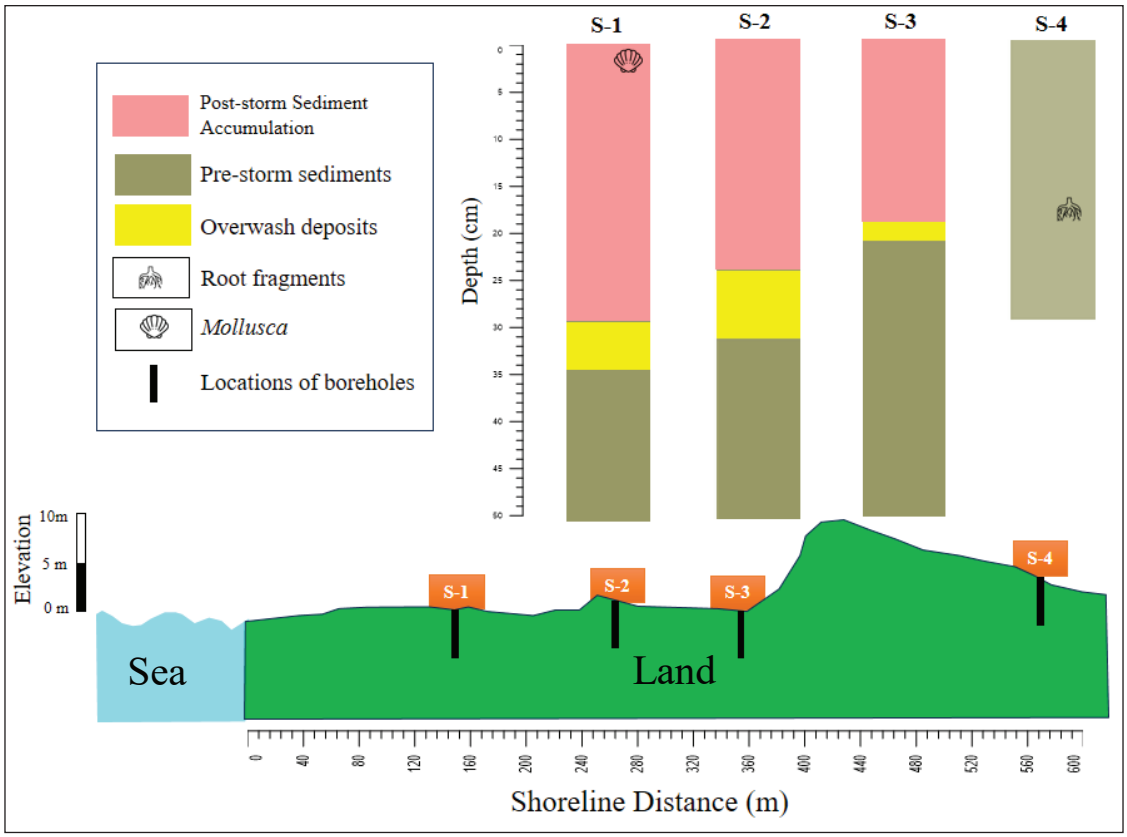

Figure 10: Schematic Representation of Over-Wash sediments from Cyclone Mora based on Textural, Geochemical and Diatom Analysis

Table 3: Lateral Variation in the Mean (μm), Sorting (σ_ϕ) and Thickness (cm) of Overwash Sediments from Kuakata and Sonadia Boreholes

Core ID	Distance from Shoreline	Mean	Sorting	Overwash Thickness
		μm	σ_ϕ	cm
Kuakata Sample Site				
K-1	50	149.5	1.70	7
K-2	144	124.6	2.01	7
K-3	375	137.0	1.81	5
K-4	Parallel to K-3	101.8	1.93	3
Sonadia Sample Site				
S-1	148	206.0	1.69	5
S-2	263	258.3	1.54	7
S-3	319	229.0	1.57	2

In contrast, Sonadia exhibits a more uniform grain size distribution, with mean particle sizes between 206.0 and 258.3 μm and moderately sorted sediments (1.54–1.69 σ_ϕ). Overwash deposit thickness in this region varies from 2 to 7 cm without a pronounced landward thinning trend. This difference is attributed to open, low-lying topography and dynamic tidal and wave influences of Sonadia Island, which promote lateral sediment dispersal rather than the directed inland transport observed in Kuakata (Hossain et al., 2023; Hoque et al., 2022; Hasan, 2020; Zheng et al., 2014).

The rates of sedimentation offer further clues about regional variations. The accretion rate at Kuakata, during the last 16 years, after the impacts of Cyclone Sidr, remained between 0.9 and 1.9 cm/year, averaging about 1.4 cm/year. This relatively low rate of sedimentation possibly signifies the stability of the beach, scarce availability of sediment, and complex interactions among oceanic forces, dominant southwest winds, and manmade elements (Bushra et al., 2021; Michels et al., 1998). The case at Sonadia, however, depicts significantly higher accretion rate, between 2.7 and 4.3 cm/year, averaging 3.5 cm/year, after Cyclone Mora in 2017. The relatively high rate of sedimentation in this area could be the result of the powerful deposition of sand through the activity of dune dynamics, in addition to the support from powerful winds, tidal activity,

contributions from rivers, and periodic current patterns (Haque et al., 2021; Hossain et al., 2023). Additionally, Aeolian activity and manmade modifications are also essential in defining the restoration and alteration of geomorphic elements in the post-cyclone environment (Javier et al., 2015; van de Graaff, 2002).

Global Insights and Local Variability in Cyclone-Induced Sediment Dynamics

The sedimentary records from Sonadia and Kuakata provide an impressive example of how overwash deposition patterns are mutually determined by coastal shape and storm intensity. Well-defined, landward-fining overwash deposits with thicknesses ranging from 3 to 7 cm were created in Kuakata by Cyclone Sidr, a Category 4 event with surges exceeding 12 m (Antony et al., 2014). These sediments extend up to 375 m inland. Similar to the findings of Haque et al. (2021), Hawkes and Horton, 2012, Hanebuth et al. (2013), and Shibayama et al. (2009), illustrates that high-energy storm surges are capable of transporting coarser sediments deeper inland until energy dissipation occurs (Table 4). Furthermore, the role of mangrove vegetation is evident through the trapping of sediments and the reduction of hydrodynamic energy (Rahman and Rahman, 2013; Baird et al., 2009; Asari et al., 2021), which not only moderates the inland penetration of overwash layers but also enriches them with organic matter.

Table 4: Comparing the Sedimentary Properties of Cyclone Sidr and Cyclone Mora, as well as Other Recent Cyclones of Comparable Strength

	Storm Surge	Cyclone Sidr	Cyclone Mora	Cyclone Sidr	Hurricane Rita	Cyclone Yasi	Typhon Haiyan
Regional Setting	**Landfall date**	Nov, 2007	May, 2017	Nov, 2007	Sept, 2007	Feb, 2011	Nov, 2013
	Location	Kuakata, Bangladesh	Sonadia, Bangladesh	Kuakata, Bangladesh	Louisiana, USA	Queensland, Australia	Samar, Philippines
	Geomorphology	Sandy Deltaic Beach	Sandy Deltaic Beach	Sandy Deltaic Beach	Beach Ridges	Sandy beach ridges	Sandy beach with reef
	Ground elevation	1-2m	0-2m	1.5-2m	0.5-2m	4-5m	1.5 to 2m
Meteorology	**Landfall Intensity**	Catagory-4	Catagory-1	Catagory-4	Catagory-3	Catagory-5	Catagory-5
	Inundation Distance	-	-	-	-	500m	2km
Sedimentary Structure	**Vertical Grading**	Type 1: White to light Grey sand Type 2: Bluish Grey Sandy Silt	Type 1: Reddish brown sand Type 2: Dark grey Sandy Silt	Unit 1: white to light grey sand Unit 2: Olive grey sandy silt	Unit 1: Sand sheet thickens upward, coarser Unit 2: washover terrace thickens upward, coarser.	Fining upward with skewed fines	Unit 1: Sand sheet thickens upward, coarser Unit 2: washover terrace thickens upward, coarser.
	Sorting	Value indicates moderate to poor condition	Value indicates moderate condition	Value indicates moderate to poor condition	Value indicates well condition	No Data	Value indicates moderate to well condition
	Lateral Grading	Fining landward except K-2	No Trend	Fining landward	Fining landward	No Trend	Fining landward
	Inland Extent	Up to 375 m	Up to 263 m	305 m	At least 500 m	Up to 87 m	350 m
	Thickness	3 to 7 cm	2 to 7 cm	5 to 55 cm	10-20cm	5-50 cm	2-50 cm
Biological properties		Dominance of freshwater and marine diatoms in wash over sediment separated from pre-storm condition	The presence of marine and fresh-water diatoms in overwash sediments separates pre-storm and post-storm layers	Diatom assemblages differentiate pre-storm and overwash sediments, showing fresh-water and marine diatoms in the latter.	Foraminifera concentration is higher in the seaward area and gradually decreases towards the land.	Marine and brackish diatoms alongside fresh-water diatoms. Higher marine percentage seaward, increased fresh-water landward	Planktic foraminifera vary with distance from shoreline
References		This study	This Study	Haque et al. (2021)	Williams (2009)	Nott et al. (2013)	Soria et al. (2017)

Cyclone Mora, a Category 1 storm with a surge height of 1–1.5 meters (Paul, 2009; IMD Mora Report, 2017), left a distinct sedimentary imprint on Sonadia Island, differing significantly from Cyclone Sidr's impact on Kuakata. Unlike well-defined, landward-thinning overwash layers from Cyclone Sidr, deposits from Cyclone Mora are more fragmented, with thicknesses ranging from 2 to 7 cm and no clear inland thinning trend. This pattern reflects low-lying, open topography of Sonadia island, which allowed the surge to spread laterally rather than penetrate deeply inland (Williams, 2009; Nott et al., 2013; Soria et al., 2017). The uniform grain size (206.0–258.3 μm) and moderate sorting (1.54–1.69 σ_ϕ) of these deposits further highlight the role of marine processes, such as tidal currents and wave action, in redistributing sediments across the island.

The presence of iron oxide-rich layers (Kabir et al., 2018) and mixed freshwater-marine diatom assemblages (Haque et al., 2021; Williams, 2010) provides additional evidence of sediment reworking during Cyclone Mora. These features suggest that even moderate cyclones can significantly alter coastal sediment dynamics, blending pre-existing terrestrial materials with storm-deposited marine sediments.

These findings emphasize that the spatial distribution and characteristics of overwash deposits are not determined solely by storm intensity. Instead, they result from the interaction between the cyclone's energy and the local coastal environment. Natural features such as mangroves, embankments, and coastal elevation play a critical role in modulating surge impacts. For instance, mangroves can trap sediments and reduce surge energy, while open, low-lying areas like Sonadia allow for broader sediment dispersion. The presence of both marine and freshwater microfossils in the deposits further confirms the dynamic mixing of sediments during cyclonic events.

CONCLUSIONS

Reconstructing past cyclones requires multiple proxy data, including sedimentary, geological, and biological evidence preserved in coastal sediments. By analyzing boreholes from the Kuakata study area, a maximum of six distinct sedimentary layers were identified, with significant cyclone-induced reworked layers ranging in thickness from 3 to 7 cm. The extent of overwash deposits in the Kuakata region reaches up to 375 m from the shoreline, with moderately sorted light grey silty sand particles. In the overwash deposits, there is a dominance of marine diatoms, along with the presence of freshwater species, which is thought to be linked to a potential storm surge combined with riverine flooding due to heavy precipitation. Post-cyclone sedimentation in the Kuakata region ranges from 0.9 cm/year to 1.9 cm/year. In the Sonadia study area, boreholes reveal a maximum of eight sedimentary layers with some distinct boundaries. The thickness of overwash deposition varies from 2 to 7 cm, characterized by a reddish-brown color and moderate sorting. The extent of sediment deposition during Cyclone Mora was 319 m from the shoreline. Post-storm sedimentation in the Sonadia region was much higher than in Kuakata, ranging from 2.7 cm/year to 4.3 cm/year. Overall, local topography, wave and tidal action, aeolian action, and vegetation play important roles in the deposition of cyclone overwash and post-cyclone sedimentation. There is a clear gap in the study of paleo-cyclones in the Bay of Bengal, particularly in understanding the sediment dynamics of different coastal zones under cyclonic influence. There is a need for studies focused on long-term sediment monitoring to understand temporal changes and post-cyclone sediment recovery, as well as investigating the impact of climate change on cyclone intensity and frequency and their subsequent effects on coastal sediment dynamics.

REFERENCES

Al Azad, A., Mita, K., Zaman, Md., Akter, M., Asik, T., Haque, A., Hussain, M., Rahman, Md. 2018. Impact of tidal phase on inundation and thrust force due to storm surge. Journal of Marine Science and Engineering 6(4), 110. doi:https://doi.org/10.3390/jmse6040110.

Alam, M.Z., Halsey, J., Haque, M.M., Talukdar, M., Moniruzzaman, M., Crump, A.R., 2018. Effect of natural disasters and their coping strategies in the Kuakata coastal belt of Patuakhali Bangladesh. Computational Water, Energy, and Environmental Engineering 07(04), 161. doi:https://doi.org/10.4236/cweee.2018.74011.

Ali, A., 1999. Climate change impacts and adaptation assessment in Bangladesh. Climate Research 12, 109–116. doi:https://doi.org/10.3354/cr012109.

Antony, C., Testut, L., Unnikrishnan, A.S., 2014. Observing storm surges in the bay of bengal from satellite altimetry. Estuarine, Coastal and Shelf Science 151, 131–140. doi:https://doi.org/10.1016/j.ecss.2014.09.012.

Antu, D.R., Islam, T.T., Ahmed, M.R., Ahmed, S., Datta, S.K., Ahmed, M.S., 2022. Diversity of bivalves and gastropods in sonadia island, Bangladesh. Bioresearch Communications 9(1), 1225–1236. doi:https://doi.org/10.3329/brc.v9i1.63603.

Anwar, Md.S., Rahman, K., Bhuiyan, M.A.E., Saha, R., 2022. Assessment of sea level and morphological changes along the eastern coast of Bangladesh. Journal of Marine Science and Engineering 10(4), 527. doi:https://doi.org/10.3390/jmse10040527.

Asari, N., Suratman, M.N., Mohd Ayob, N.A., Abdul Hamid, N.H., 2021. Mangrove as a natural barrier to environmental risks and coastal protection. In: R.P. Rastogi, M. Phulwaria and D.K. Gupta, eds., Mangroves: Ecology, Biodiversity and Management. pp.305–322. doi:https://doi.org/10.1007/978-981-16-2494-0_13.

Baird, A.H., Bhalla, R.S., Kerr, A.M., Pelkey, N.W., Srinivas, V., 2009. Do mangroves provide an effective barrier to storm surges? Proceedings of the National Academy of Sciences 106(40), 111–E111. doi:https://doi.org/10.1073/pnas.09008799106.

Bangladesh Tourism Board, 2023. Kuakata. [online] beautifulbangladesh.gov.bd. Available at: https://beautifulbangladesh.gov.bd/cat/spring/20 [Accessed 17 Sep. 2023].

Banglapedia, 2021. Bangladesh: cyclonic storm tracks. Available at: https://en.banglapedia.org/index.php/File:Cyclone.jpg [Accessed 19 Sep. 2023].

Bennington, J.B., Farmer, E.C., 2014. Recognizing past storm events in sediment cores based on comparison to recent overwash sediments deposited by superstorm sandy. In: J.B. Bennington and E.C. Farmer, eds., Learning from the Impacts of Superstorm Sandy. [online] Academic Press, pp.89–106. doi:https://doi.org/10.1016/B978-0-12-801520-9.00007-9.

Blott, S.J., Pye, K., 2001. GRADISTAT: a grain size distribution and statistics package for the analysis of unconsolidated sediments. Earth Surface Processes and Landforms 26(11), 1237–1248. doi:https://doi.org/10.1002/esp.261.

Brammer, H., 2014. Bangladesh's dynamic coastal regions and sea-level rise. Climate Risk Management 1, 51–62. doi:https://doi.org/10.1016/j.crm.2013.10.001.

Bushra, N., Mostafiz, R.B., Rohli, R.V., Friedland, C.J., Rahim, M.A., 2021. Technical and social Approaches to study shoreline change of Kuakata, Bangladesh. Frontiers in Marine Science 8. doi:https://doi.org/10.3389/fmars.2021.730984.

Cahoon, D.R., 2006. A review of major storm impacts on coastal wetland elevations. Estuaries and Coasts [online] 29(6), 889–898. Available at: https://www.jstor.org/stable/4124818 [Accessed 29 May 2024].

Coch, N.K., 1994. Geologic effects of hurricanes. Geomorphology 10(1-4), 37–63. doi:https://doi.org/10.1016/0169-555x(94)90007-8.

Das, O., Wang, Y., Donoghue, J., Xu, X., Coor, J., Elsner, J., Xu, Y., 2013. Reconstruction of paleostorms and paleoenvironment using geochemical proxies archived in the sediments of two coastal lakes in northwest Florida. Quaternary Science Reviews [online] 68, 142–153. doi:https://doi.org/10.1016/j.quascirev.2013.02.014.

Dasgupta, S., Laplante, B., Murray, S., Wheeler, D., 2009. Climate change and the future impacts of storm-surge disasters in dveloping countries. SSRN Electronic Journal. doi:https://doi.org/10.2139/ssrn.1479650.

Deb, M., Ferreira, C.M., 2017. Potential impacts of the Sunderban mangrove degradation on future coastal flooding in Bangladesh. Journal of Hydro-environment Research 17, 30–46. doi:https://doi.org/10.1016/j.jher.2016.11.005.

Donnelly, C., Kraus, N., Larson, M., 2006. State of knowledge on measurement and modeling of coastal overwash. Journal of Coastal Research 224, 965–991. doi:https://doi.org/10.2112/04-0431.1.

Dufois, F., Lowe, R.J., Branson, P., Fearns, P., 2017. Tropical cyclone-driven sediment dynamics over the Australian north west shelf. Journal of Geophysical Research: Oceans 122(12), 10225–10244. doi:https://doi.org/10.1002/2017jc013518.

Emanuel, K., 2003. Tropical cyclones. Annual Review of Earth and Planetary Sciences 31(1), 75–104. doi:https://doi.org/10.1146/annurev.earth.31.100901.141259.

Folk, R.L., Ward, W.C., 1957. Brazos river bar [Texas]; a study in the significance of grain size parameters. Journal of Sedimentary Research [online] 27(1), 3–26. doi:https://doi.org/10.1306/74d70646-2b21-11d7-8648000102c1865d.

Gresham, C.A., Williams, T.M., Lipscomb, D.J., 1991. Hurricane hugo wind damage to southeastern U.S. coastal forest tree species. Biotropica 23(4), 420. doi:https://doi.org/10.2307/2388261.

Hache, I., Karius, V., von Eynatten, H., 2021. Storm surge induced sediment accumulation on marsh islands in the southeastern north sea: Implications for coastal protection. Estuarine, Coastal and Shelf Science 263, 107629. doi:https://doi.org/10.1016/j.ecss.2021.107629.

Hanebuth, T.J.J., Kudrass, H.R., Linstadter, J., Islam, B., Zander, A.M., 2013. Rapid coastal subsidence in the central Ganges-Brahmaputra delta (Bangladesh) since the 17th century deduced from submerged salt-producing kilns. Geology 41(9), 987–990. doi:https://doi.org/10.1130/g34646.1.

Haque, M.M., Yamada, M., Uchiyama, S., Hoyanagi, K., 2021. Depositional setup and haracteristics of the storm deposit by the 2007 cyclone sidr on Kuakata coast, Bangladesh. Marine Geology 442, 106652. doi:https://doi.org/10.1016/j.margeo.2021.106652.

Hasan, G.M.J., Matin, N., 2019. Estimation of areal changes along the coastline of Bangladesh due to erosion and accretion. International Journal of Engineering Sciences 12(3). doi:https://doi.org/10.36224/ijes.120305.

Hasan, S., 2020. Optimized energy system design and analysis for Sonadia island. In: 2020 2nd International Conference on Sustainable Technologies for Industry 4.0 (STI). pp.1–6. doi:https://doi.org/10.1109/STI50764.2020.9350451.

Hawkes, A.D., Horton, B.P., 2012. Sedimentary record of storm deposits from Hurricane Ike, Galveston and San Luis Islands, Texas. Geomorphology 171-172, 180–189. doi:https://doi.org/10.1016/j.geomorph.2012.05.017.

Heller, C.A., Michelutti, N., Burn, M.J., Palmer, S.E., Smol, J.P., 2021. The response of diatom assemblages in a Jamaican coastal lagoon to Hurricane and drought activity over the past millennium. The Holocene 31(9), 1359–1365. doi:https://doi.org/10.1177/09596836211019095.

Hong, I., Pilarczyk, J.E., Horton, B.P., Fritz, H.M., Kosciuch, T.J., Wallace, D.J., Dike, C., Rarai, A., Harrison, M.J., Jockley, F.R., 2018. Sedimentological characteristics of the 2015 tropical cyclone pam overwash sediments from Vanuatu, south pacific. Marine Geology 396, 205–214. doi:https://doi.org/10.1016/j.margeo.2017.05.011.

Hoque, E., Chowdhury, S.R., Chowdhury, Z.R., Uddin, M.M., Alam, M.S., Karmakar, S., 2022. Remote sensing measures of sandbars along the shoreline of Sonadia island, Bangladesh, 1972–2006. In: J.G. Lyon and L. Lyon, eds., Geospatial Information Handbook for Water Resources and Watershed Management Fundamentals and Analyses. Boca Raton: CRC Press, pp.113–128. doi:https://doi.org/10.1201/9781003175018-7.

Hossain, M.S., Islam, M.A., Badhon, F.F., Imtiaz, T., 2021a. Hydrometer analysis. [online] mavs open press. Available at: https://uta.pressbooks.pub/soilmechanics/chapter/hydrometer-analysis/ [Accessed 13 Sep. 2023].

Hossain, M.S., Islam, M.A., Badhon, F.F., Imtiaz, T., 2021b. Sieve analysis. [online] mavs open press. Available at: https://uta.pressbooks.pub/soilmechanics/chapter/sieve-analysis/ [Accessed 13 Sep. 2023].

Hossain, M.S., Yasir, M., Shahriar, M.S., Jahan, M., Liu, S., Niang, A.J., 2023. Morphological change assessment of a coastal island in SE Bangladesh reveal high accumulation rates. Regional Studies in Marine Science 62,v102969–102969. doi:https://doi.org/10.1016/j.rsma.2023.102969.

Huq, S.M.I., Alam, M.D., 2005. A handbook on analyses of soil, plant, and water. BACER-DU, University of Dhaka, pp.1–242.

Hussain, N., Khan, E., 2018. Coastline dynamics and raising landform: a geo-informatics based study on the bay of bengal, Bangladesh. Indonesian Journal of Geography 50(1), 41–41. doi:https://doi.org/10.22146/ijg.26655.

IMD Mora Report, 2017. Severe cyclonic storm, 'MORA' over the bay of bengal (28–31 May 2017). [online] New Delhi, India: Cyclone warning division. Available at: https://rsmcnewdelhi.imd.gov.in/uploads/report/26/26_385d6a_mora.pdf [Accessed 19 Sep. 2023].

Islam, A.S., Bala, S.K., Hussain, M.A., Hossain, M.A., Rahman, M.M., 2011. Performance of coastal structures during cyclone sidr. Natural Hazards Review 12(3), 111–116. doi:https://doi.org/10.1061/(asce)nh.1527-6996.0000031.

Islam, M.S., Tooley, M.J., 1999. Coastal and sea-level changes during the holocene in Bangladesh. Quaternary International 55(1), 61–75. doi:https://doi.org/10.1016/s1040-6182(98)00025-1.

Islam, T., Peterson, R.E., 2008. Climatology of landfalling tropical cyclones in Bangladesh 1877–2003. Natural Hazards 48(1), 115–135. doi:https://doi.org/10.1007/s11069-008-9252-4.

Javier, D.J., Veiga, E.M., Esteban, V., 2015. Effects of climate change on coastal evolution. In: G. Lollino, A. Manconi, J. Clague, W. Shan and M. Chiarle, eds., Engineering Geology for Society and TerritoryVolume 1. Cham: Springer International Publishing, pp.395–399.

Kabir, M., Deeba, F., Majumder, R., Khalil, M., Islam, M., 2018. Heavy mineral distribution and geochemical studies of coastal sediments at Sonadia island, Bangladesh. Nuclear Science and Application 27, 2.

Kjeldahl, J., 1883. Neue methode zur bestimmung des stickstoffs in organischen körpern. fresenius' zeitschrift für analytische chemie 22(1), 366–382. doi:https://doi.org/10.1007/bf01338151.

Kosciuch, T.J., Pilarczyk, J.E., Hong, I., Fritz, H.M., Horton, B.P., Rarai, A., Harrison, M.J., Jockley, F.R., 2018. Foraminifera reveal a shallow nearshore origin for overwash sediments deposited by tropical cyclone pam in vanuatu (South Pacific). Marine Geology 396, 171–185. doi:https://doi.org/10.1016/j.margeo.2017.06.003.

Lambert, W.J., Aharon, P., Rodriguez, A.B., 2007. Catastrophic hurricane history revealed by organic geochemical proxies in coastal lake sediments: a case study of lake Shelby, Alabama (USA). Journal of Paleolimnology 39(1), 117–131. doi:https://doi.org/10.1007/s10933-007-9101-6.

Meyers, P.A., 1997. Organic geochemical proxies of paleoceanographic, paleolimnologic, and paleoclimatic processes. Organic Geochemistry 27(5-6), 213–250. doi:https://doi.org/10.1016/s0146-6380(97)00049-1.

Michels, K.H., Kudrass, H.R., Hübscher, C., Suckow, A., Wiedicke, M., 1998. The submarine delta of the Ganges–Brahmaputra: cyclone-dominated sedimentation patterns. Marine Geology 149(1-4), 133–154. doi:https://doi.org/10.1016/s0025-3227(98)00021-8.

MoFDM, 2008. Super cyclone sidr 2007 impacts and strategies for interventions. [online] Bangladesh secretariat, Dhaka, Bangladesh: Ministry of food and disaster management, Government of People's Republic of Bangladesh, pp.1–56. Available at: https://www.preventionweb.net/files/9470_cyclonebangladesh.pdf [Accessed 17 Sep. 2023].

Morton, R.A., Goff, J.R., Nichol, S.L., 2008. Hydrodynamic implications of textural trends in sand deposits of the 2004 tsunami in Sri Lanka. Sedimentary Geology 207(1-4), 56–64. doi:https://doi.org/10.1016/j.sedgeo.2008.03.008.

Muller, J., Collins, J.M., Gibson, S., Paxton, L., 2017. Recent advances in the emerging field of paleotempestology. In: J.M. Collins and K. Walsh, eds., Hurricanes and Climate Change. Springer Cham, pp.1–33. doi:https://doi.org/10.1007/978-3-319-47594-3_1.

Nott, J., Chague-Goff, C., Goff, J., Sloss, C., Riggs, N., 2013. Anatomy of sand beach ridges: Evidence from severe tropical cyclone yasi and its predecessors, Northeast Queensland, Australia. Journal of Geophysical Research: Earth Surface 118(3), 1710–1719. doi:https://doi.org/10.1002/jgrf.20122.

Paul, B.K., 2009. Human injuries caused by Bangladesh's cyclone sidr: an empirical study. Natural Hazards 54(2), 483–495. doi:https://doi.org/10.1007/s11069-009-9480-2.

Rahman, Md.A., Rahman, Md.A., 2013. Effectiveness of coastal bio-shield for reduction of the energy of storm surges and cyclones. Procedia Engineering 56, 676–685. doi:https://doi.org/10.1016/j.proeng.2013.03.177.

Sarwar, M.G.M., Woodroffe, C.D., 2013. Rates of shoreline change along the coast of Bangladesh. Journal of Coastal Conservation 17(3), 515–526. doi:https://doi.org/10.1007/s11852-013-0251-6.

Shibayama, T., Tajima, Y., Kakinuma, T., Nobuoka, H., Yasuda, T., Ahsan, R., Rahman, M., Islam, M.S., 2009. Field survey of storm surge disaster due to cyclone sidr in Bangladesh. In: Proceedings of coastal dynamics. Coastal dynamics 2009 - impacts of human activities on dynamic coastal processes. pp.1–8. doi:https://doi.org/10.1142/9789814282475_0128.

Sikder, M.B., Chowdhury, P., Akter, S.A., Kabir, M.N., Rawfu, R.N., 2021. Geomorphic characteristics of coastal beach using geospatial techniques: a case study of Kuakata beaches, Bangladesh. Bangladesh Maritime Journal (BMJ) [online] (Special), 225–240. Available at: https://bsmrmu.edu.bd/public/files/econtents/61a4516038918MS%20-%2014%20A.pdf [Accessed 17 Sep. 2023].

Smith, A.W., Jackson, L.A., 1990. Assessment of the past extent of cyclone beach erosion. Journal of Coastal Research [online] 6(1), 73–86. Available at: https://www.jstor.org/stable/4297646.

Soria, J.L.A., Switzer, A.D., Pilarczyk, J.E., Tang, H., Weiss, R., Siringan, F., Manglicmot, M., Gallentes, A., Lau, A.Y.A., Cheong, A.Y.L., Koh, T.W.L., 2018. Surf beat-induced overwash during typhoon haiyan deposited two distinct sediment assemblages on the carbonate coast of hernani, samar, central Philippines. Marine Geology 396, 215–230. doi:https://doi.org/10.1016/j.margeo.2017.08.016.

Tebaldi, C., Strauss, B.H., Zervas, C.E., 2012. Modelling sea level rise impacts on storm surges along US coasts. Environmental Research Letters 7(1), p.014032. doi:https://doi.org/10.1088/1748-9326/7/1/014032.

Troels-Smith, J., 1955. Characterization of unconsolidated sediments. Reitzels Forlag.

Tweel, A.W., Turner, R.E., 2012. Landscape-scale analysis of wetland sediment deposition from four tropical cyclone events. PLoS ONE 7(11), p.e50528. doi:https://doi.org/10.1371/journal.pone.0050528.

van de Graaff, J., 2002. Coastal protection, structures and (Sea) Dikes. In: J. Chen, D. Eisma, K. Hotta and W.H. Jesse, eds., Engineered Coasts. [online] Springer Netherlands, 229–247. Available at: https://doi.org/10.1007/978-94-017-0099-3_11.

Walkley, A., Black, I.A., 1934. An examination of the degtjareff method for determining soil organic matter, and a proposed modification of the chromic acid titration method. Soil Science 37(1), 29–38. doi:https://doi.org/10.1097/00010694-193401000-00003.

Wang, L., Bianchette, T.A., Liu, K., 2019. Diatom evidence of a paleohurricane-induced coastal flooding event in weeks bay, Alabama, USA. Journal of Coastal Research [online] 35(3), 499–508. Available at: https://www.jstor.org/stable/26626083.

Wasimi, S.A., 2009. Statistical forecasting of tropical cyclones for Bangladesh. In: Y. Charabi, ed., Indian ocean tropical cyclones and climate change. Springer eBooks, pp.131–141. doi:https://doi.org/10.1007/978-90-481-3109-9_17.

Williams, H.F.L., 2009. Stratigraphy, sedimentology, and microfossil content of hurricane rita storm surge deposits in southwest louisiana. Journal of Coastal Research 254, 1041–1051. doi:https://doi.org/10.2112/08-1038.1.

Williams, H.F.L., 2010. Storm surge deposition by hurricane Ike on the mcfaddin national wildlife refuge, texas: Implications for paleotempestology studies. The Journal of Foraminiferal Research 40(3), 210–219. doi:https://doi.org/10.2113/gsjfr.40.3.210.

Williams, H.F.L., Flanagan, W.M., 2009. Contribution of hurricane rita storm surge deposition to long-term sedimentation in Louisiana coastal Woodlands and Marshes. Journal of Coastal Research [online] 1671–1675. Available at: https://www.jstor.org/stable/25738074 [Accessed 29 May 2024].

Zheng, Y., Chen, J., Tao, Z., 2014. Distribution characteristics of the intensity and extreme intensity of tropical cyclones influencing China. Journal of Meteorological Research 28(3), 39–406. doi:https://doi.org/10.1007/s13351-014-3050-6.